Zinc Inhibition of Bacterial Cytochrome bc(1) Reveals the Role of Cytochrome b E295 in Proton Release at the Q(o) Site

ARTICLE *in* BIOCHEMISTRY · MAY 2011

Impact Factor: 3.02 · DOI: 10.1021/bi200230e · Source: PubMed

8 AUTHORS, INCLUDING:

Barbara Zambelli
University of Bologna
41 PUBLICATIONS **701** CITATIONS
SEE PROFILE

Stefano Ciurli
University of Bologna
141 PUBLICATIONS **3,409** CITATIONS
SEE PROFILE

Giovanni Venturoli
University of Bologna
110 PUBLICATIONS **1,941** CITATIONS
SEE PROFILE

Fevzi Daldal
University of Pennsylvania
181 PUBLICATIONS **6,095** CITATIONS
SEE PROFILE

Published in final edited form as:
Biochemistry. 2011 May 24; 50(20): 4263–4272. doi:10.1021/bi200230e.

Zinc inhibition of bacterial cytochrome bc_1 reveals the role of cytochrome *b* E295 in proton release at the Q_o site†

Dong-Woo Lee[1,5], **Youssef El Khoury**[2], **Francesco Francia**[3], **Barbara Zambelli**[4], **Stefano Ciurli**[4], **Giovanni Venturoli**[3], **Petra Hellwig**[2], and **Fevzi Daldal**[1,*]

[1]Department of Biology, University of Pennsylvania, Philadelphia, PA19104, USA

[2]Institut de Chimie, UMR 7177, Laboratoire de Spectroscopie Vibrationnelle et Electrochimie des Biomolécules, Université de Strasbourg, 67070 Strasbourg, France

[3]Laboratorio di Biochimica e Biofisica, Dipartimento di Biologia, Università di Bologna, 40126 Bologna, Italy

[4]Laboratory of Bioinorganic Chemistry, University of Bologna, 40127 Bologna, and Center for Magnetic Resonance, University of Florence, Italy

Abstract

The cytochrome (cyt) bc_1 complex (cyt bc_1) plays a major role in the electrogenic extrusion of protons across the membrane responsible for the proton motive force to produce ATP. Proton-coupled electron transfer underlying the catalysis of cyt bc_1 is generally accepted, but the molecular basis of coupling and associated proton efflux pathway(s) remains unclear. Herein we studied Zn^{2+}-induced inhibition of *Rhodobacter capsulatus* cyt bc_1 using enzyme kinetics, isothermal titration calorimetry (ITC) and electrochemically-induced FTIR difference spectroscopy with the purpose to understand the Zn^{2+}-binding mechanism and its inhibitory effect on cyt bc_1 function. Analogous studies were carried out on a mutant of cyt *b*, E295, a residue previously proposed to bind Zn^{2+} on the basis of extended X-ray absorption fine-structure spectroscopy. ITC analysis indicated that mutation of E295 into valine, a non-coordinating residue, results in the reduction of Zn^{2+}-binding affinity. The kinetic study showed that wild-type cyt bc_1 and its E295V mutant have similar levels of apparent K_m values for decylbenzohydroquinone as a substrate (4.9 ± 0.2 μM and 3.1 ± 0.4 μM, respectively), whereas their K_I values for Zn^{2+} are 8.3 μM and 38.5 μM, respectively. The calorimetry-based K_D values for the high affinity site of cyt bc_1 are of the same order of magnitude as the K_I values derived from the kinetic analysis. Furthermore, the FTIR signal of protonated acidic residues was perturbed in the presence of Zn^{2+}, whereas the E295V mutant exhibited no significant change in electrochemically induced FTIR difference spectra measured in the presence and absence of Zn^{2+}. Our overall results indicate that the proton-active E295 residue near the Q_o site of cyt bc_1 can bind directly to Zn^{2+}, resulting in a decrease of the electron transferring activity without changing drastically the redox potentials of the cofactors of the enzyme. We conclude that E295 is involved in proton efflux coupled to electron transfer at the Q_o site of cyt bc_1.

†This work is supported by grants to F.D. from NIH (GM 38237) and DOE (91ER 20052). The VP-ITC instrument is the property of CIRB-UniBO. G.V. and F.F. acknowledge financial support of MIUR of Italy (grants PRIN 2008 ZWHZJT and PRIN 2008 XB774B), and P.H. and Y.E.K acknowledge financial support from the ANR Chaire d'Excellence and CNRS.

*To whom correspondence should be addressed: Tel: (215) 898-4394. Fax: (215) 898-8780. fdaldal@sas.upenn.edu.
[5]**Current addresses**: Industrial Biotechnology and Bioenergy Research Center, Korea Research Institute of Bioscience and Biotechnology, Daejeon, Korea 305-806.

Keywords

Cytochrome bc_1; Zinc inhibition; *Rhodobacter capsulatus*; cytochrome *b* mutations; Proton efflux; Electron Transport Chain

In the respiratory and photosynthetic chains of organisms, electrons are transferred sequentially from low redox potential donors to high redox potential acceptors, in events coupled to proton translocation across the membrane. The process maintains a transmembrane electrochemical proton gradient (ΔpH), which is used to drive the synthesis of ATP (1, 2). The concerted movement of protons and electrons is a common feature of many energy-transducing complexes including the photosynthetic reaction center (RC), cytochrome (cyt) bc_1 complex (cyt bc_1), and cyt *c* oxidase (Cox). Among them, cyt bc_1 is one of the components that generates a proton gradient across the membrane by the uptake and release of protons on both sides of the lipid bilayer in a manner coupled to electron transfer (3, 4). According to the Q cycle mechanism, a hydroquinone (QH_2) molecule is oxidized at a QH_2-oxidizing (Q_o) site of cyt bc_1 to produce two electrons. The first electron goes to the high-potential chain comprised of the Rieske Fe/S protein and cyt c_1, while the other electron enters into a low-potential chain fully confined to cyt *b* hemes b_L and b_H (5–8). Eventually, the high-potential chain in phototrophic bacteria conveys the first electron from QH_2 to a terminal acceptor (*i.e.*, either Cox in respiration or photo-oxidized RC in photosynthesis) via the cyt c_2 (and cyt c_y in *Rhodobacter capsulatus*) (9–11). The second electron from QH_2 is transferred to the Q_i site via the two hemes b_L and b_H to reduce a Q to an intermediate SQ (3, 12). Upon the oxidation of a second QH_2 at a Q_o site, another electron is used to reduce the SQ at the Q_i site to QH_2. Consequently, a complete turnover of cyt bc_1 consumes one Q and two protons at the *n* side of the membrane to generate a QH_2 concomitantly with oxidation of two QH_2 at the Q_o site(s) to release four protons to the *p* side of the membrane, resulting in the formation of a proton gradient (ΔpH) and a membrane potential ($\Delta\psi$) across membrane. The bifurcated electron transfer reaction at the Q_o site between the high- and low-potential chains of the enzyme is a unique functional characteristic of cyt bc_1 through which the free energy difference between the Q_{pool} and the electron acceptor is used to generate ΔpH and $\Delta\psi$. Protons are known to move through ordered chains of water, but how the rate and direction of proton movement is controlled and coordinated with coupled electron transfer is not understood. Particularly, little is known about the proton uptake and release events of cyt bc_1.

Several approaches have been used to determine the proton transfer pathway(s), starting with cyt *b*, which plays a key role in both electron transfer and proton release and uptake activities (13–15). Initially, the use of dicyclohexylcarbodiimide (DCCD), a well-known carboxyl-modifying reagent, suggested that the cyt *b* D187 residue of *R. sphaeroides* cyt bc_1 might be involved in proton translocation (13). Subsequent studies (15) demonstrated that this residue was unlikely to be involved in the protonogenic reactions of cyt bc_1. Rather, DCCD caused inhibition of the Fe/S protein-mediated electron transfer reactions between the Q_o site and cyt c_1 as well as the QH_2 oxidation at the Q_o site (14). Molecular modeling studies of the DCCD-treated cyt bc_1 proposed that conformational changes by DCCD binding to E163 (mitochondrial numbering) in the *cd*2 loop of cyt *b* of chicken cyt bc_1 could generate new hydrogen bonds between E272 and D253 and Y274 residues to affect the rotation and protonation of E272 (corresponding to *R. capsulatus* E295) (16), which was pointed out to be important to capture a proton derived from QH_2 oxidation at the Q_o site (17). Nevertheless the proton transfer pathway in the bacterial cyt bc_1 still remains unclear.

Earlier observations have indicated that transition metal ions such as Zn^{2+} and Cd^{2+} can inhibit the proton transfer activity of bacterial RC (18–20). When Zn^{2+} binds to the RC, the

rate of proton transfer to E212 of the RC subunit L was decreased, becoming a rate-limiting step (20). In addition, the X-ray crystal structure of the RC bound with Zn^{2+} revealed that the Zn^{2+} binding cluster D124, H126 and H128 of the RC subunit H were involved in the pathway of the first proton delivery to Q_B^- at the entry point (21). Furthermore, the second proton supplied to $(Q_BH)^-$ by E212 also share the same entry point of the first proton, close to the metal binding cluster (20). Similarly, the proton uptake pathways (*i.e.*, the D and K channels) in the Cox were studied using Zn^{2+} and Cd^{2+} binding experiments (22, 23). These and other related works indicated that determination of transition metal binding sites in energy transducing components provides an incisive approach to identify the residues involved in proton transfer pathways. Previously, we probed the local structure of Zn^{2+} bound stoichiometrically to non-crystallized cyts bc_1 purified from bacteria and mitochondria using Zn K-edge extended X-ray absorption fine-structure spectroscopy(EXAFS) (24), which provided results consistent with the crystal structures of the same cyts bc_1 bound with Zn^{2+} (25). EXAFS data demonstrated that the *R. capsulatus* cyt bc_1 Zn^{2+}-binding site exhibited a distinct hexa-coordination and pseudo-octahedral geometry, which included the residues H276, D278, N279, and E295. This binding mode is different from the four-coordinate tetrahedral Zn^{2+}-binding site observed in the mitochondrial cyts bc_1, but remarkably, the locus of metal ion binding was identical (Fig. 1). The metal-binding residues are close to the *p* side of the membrane surface, suggesting that this locus could represent the proton exit domain(s) of the Q_o site. In the light of the earlier works suggesting that mitochondrial E272 (E295 in *R. capsulatus* cyt bc_1) is tightly involved in QH_2 oxidation (17, 26), we examined the effect of Zn^{2+}-binding to cyt bc_1. We carried out inhibitory kinetics, isothermal titration calorimetry analyses, and electrochemically-induced FTIR difference spectroscopy for the wild-type enzyme and its E295V mutant variant in the presence and absence of Zn^{2+}. Our overall findings indicate that the Zn^{2+} binding ligand E295 of cyt *b* affects the catalytic activity (*i.e.*, k_{cat}) of cyt bc_1, suggesting that it modulates rapid electron transfer in a manner coupled to proton release from the Q_o site of the enzyme.

Materials and Methods

Growth conditions and purification of cyt bc_1

R. capsulatus strains were grown at 35 °C in mineral-peptone-yeast extract (MPYE) enriched medium supplemented with 10 μg/mL kanamycin under semiaerobic/dark respiratory conditions (27). The wild-type and mutant cyt bc_1, as well as the two-subunit cyt b-c_1 subcomplex lacking the Fe/S protein enzymes were purified from chromatophore membranes derived from cells grown under the respiratory conditions as described previously (28, 29). Briefly, chromatophore membranes prepared in 50 mM Tris-HCl buffer (pH 8.0) and 100 mM NaCl were solubilized with dodecyl maltoside (DDM) to a final concentration of 1 mg DDM per mg of total proteins. The mixture was stirred gently for 1 h at 4 °C, and then ultra-centrifuged (120,000 × g for 2 h) to eliminate non-dispersed membranes. The supernatant was loaded onto a DEAE-Biogel A column (2.6 × 32 cm) pre-equilibrated with 50 mM Tris-HCl buffer (pH 8.0) containing 20% glycerol, 0.01% (w/v) DDM, and 100 mM NaCl (Buffer A). The column was washed with 5 to 6 column volumes (CVs) of Buffer A containing 150 mM NaCl, and then the remaining photosynthetic pigments were washed with 3 to 4 CVs of the same buffer until a red band on top of the column became visible. The adsorbed cyt bc_1 proteins were eluted with 4 CVs of a linear 150–400 mM NaCl gradient in the presence of 0.01% (w/v) DDM. Fractions were monitored for their absorption at 280 and 420 nm, and 500 to 600 nm for their dithionite-reduced *minus* ferricyanide-oxidized optical difference spectra, and those containing the highest concentrations of *c*- and *b*-type cyts were pooled and concentrated using an Amicon Diaflo apparatus equipped with a PM30 membrane. The concentrated sample (~2 mL) was

passed through a Sephacryl S400 size-exclusion column (405 mL), pre-equilibrated with 10 CVs of 50 mM Tris-HCl buffer (pH 8.0) containing 150 mM NaCl, 20% glycerol, and 0.01% (w/v) DDM. Fractions containing cyt bc_1 were pooled, concentrated using Amicon Ultra (50K MW cut off) centrifugal filter devices (Millipore Co., Ireland), and stored at −80 °C in the presence of 20% glycerol until further use. The concentration of cyt bc_1 was estimated from reduced *minus* oxidized difference spectra with an extinction coefficient of 28.5 mM^{-1} cm^{-1} for the dithionite-reduced cyt *b* (at 560 nm versus 570 nm) (29). Protein concentrations were determined using the bicinchoninic acid method (30) with bovine serum albumin as a standard. SDS-PAGE (15%) were run as described in (31), and prior to loading, samples were solubilized in 62.5 mM Tris (pH 6.8), 2% SDS, 0.1 M dithiothreitol, 25% glycerol, and 0.01% bromophenol blue with subsequent incubation at 60 °C for 10 min.

Enzyme kinetics

Decylbenzohydroquinone (DBH_2):cyt reductase assays were performed as described in (29). Reaction mixtures (2 mL) contained 50 mM sodium phosphate buffer (pH 7.4), 40 μM horse heart cyt *c*, 2 mM KCN, 0.1 g/L DDM, and 2.3 nM purified cyt bc_1. Reductase reaction was started by addition of DBH_2 in dimethyl sulfoxide (final concentration 40 μM). Michaelis-Menten kinetics was performed as above in a stirred cuvette thermostatted at 20 °C using various concentrations of DBH_2 as a substrate ranging from 0.5 to 40 μM. The decylbenzoquinone (DB) concentration was determined spectroscopically using an extinction coefficient of 16 mM^{-1} cm^{-1}, and the solution is fully reduced with sodium borohydride (32). For Zn^{2+} inhibition kinetics, up to 0.2 mM $ZnSO_4$ from stock solutions of 0.1, 1, 10, or 100 mM (2 to 10 μL) was added to the reaction mixtures containing 2.3 nM purified cyt bc_1 in a stirred cuvette to give the desired final concentration and pre-incubated for 1 min before starting the reaction by addition of 40 μM DBH_2. Thereafter, the reduction of cyt *c* was monitored at 550 nm for 1 min to yield an initial rate of enzyme reaction. One unit of cyt bc_1 activity was defined as the amount of enzyme that produced 1 μmole of reduced cyt *c* per min under the assay conditions.

Isothermal Titration Calorimetry (ITC) analysis

Zn^{2+} titration experiments were performed at 25°C using a high-sensitivity VP-ITC microcalorimeter (MicroCal LLC, Northampton, MA). The $ZnSO_4$ solutions were prepared in 50 mM Tris-HCl buffer (pH 8.0) containing 150 mM NaCl, 20% glycerol, and 0.01% (w/v) DDM to final concentrations ranging from 350 to 700 μM. The reference cell was filled with deionized water. Each experiment was started with a small injection of 1–2 μL, which was discarded from the analysis of the integrated data, in order to avoid artifacts due to the diffusion through the injection port occurring during the long equilibration period, locally affecting the protein concentration near the syringe needle tip. Care was taken to start the first addition after baseline stability had been achieved. In each individual titration, 5 μL of the $ZnSO_4$ solution were injected into a solution of the wild-type and E295V mutant cyt bc_1 (10–12 μM) diluted in the same buffer using a computer-controlled 310 μL micro-syringe. Allowing a time-interval of 300 s between each Zn^{2+} injection ensured chemical equilibrium of the system. For a control experiment, the metal solution without enzyme was titrated under the same conditions. Integrated heat data were fitted by a nonlinear least-square minimization algorithm using the MicroCal Origin software.

FTIR spectroscopic analysis

FTIR difference spectra were recorded as a function of the applied potential using Vertex 70 spectrometer (Bruker Optics, Germany) equipped with an MCT detector and a globar light source. The difference spectra were recorded in the 1800-800 cm^{-1} range using a previously described electrochemical cell (33). Although using ZnSe windows instead of CaF_2 allow recording the difference spectra from 1800-650 cm^{-1}, here the spectra were recorded

between 1800-800 cm^{-1} (34). In order to accelerate the redox reaction, a mixture of mediators was used as described (35). The protein was equilibrated at an initial electrode potential, and a single-beam spectrum was recorded. Then the final potential was applied, and a single-beam spectrum was again recorded after equilibration. Equilibration generally took less than 10 min for the full potential step from −0.292 to +0.708 V vs. SHE. The difference spectra presented here were calculated from two single-beam spectra, with the initial spectrum taken as reference. Typically, 2×256 interferograms at 4 cm^{-1} resolution were co-added for each single-beam spectrum, and Fourier-transformed using triangular apodization and a zero-filling factor of 2. At least, 35 difference spectra were averaged.

UV/Vis spectroscopic analysis

The UV/Vis difference spectra of all the samples were recorded on a Cary 300 spectrometer using the same electrochemical cell as for the FTIR difference spectroscopy equipped with CaF_2 windows. The UV-Vis potentiometic oxidative titrations of the cyt bc_1 samples were performed by following the evolution of the Soret band of the hemes absorbance. The absorbance values were then plotted *versus* the applied potential.

Results

Kinetics of wild-type and cyt b E295V mutant cyt bc_1

The kinetic parameters of wild-type cyt bc_1 were studied and compared with its E295V mutant derivative. First, to establish the ratio of enzyme *versus* substrate (*i.e.*, cyt bc_1 *vs* DBH_2) necessary to have a reliable initial velocity, we monitored the reduction of horse heart cyt *c* (the electron acceptor) at different concentrations of DBH_2 (the electron donor) at 550 nm under standard assay conditions. The study demonstrated that both the wild-type enzyme and its E295V mutant showed good linearity of the reaction rate over 1 min interval using a [S]/[E] ratio of $>10^6$. We analyzed the kinetic data to determine the K_m values for DBH_2 and V_{max} using double reciprocal plots as well as fitting data with a simple Michaelis-Menten equation (Table 1). The wild-type cyt bc_1 featured a K_m of 4.9 μM for DBH_2 as a substrate, and a V_{max} value of 42.4 μmol min^{-1} mg^{-1}. The E295V mutant showed a slightly lower K_m value (3.1 μM) as compared to the wild type. This value is similar to the case of the E272Q of yeast cyt bc_1 (3.2 μM) (36), and is slightly lower than that of the yeast cyt bc_1 E272V mutant of (4.2 μM) (37), indicating that the E295V mutation does not cause any significant difference in the QH_2 binding affinity, a finding which is consistent with previous EPR data of different E295 mutants (26). It has been shown, using light-activated kinetics with chromatophore membranes derived from *R. capsulatus*, that the E295V mutant exhibits about 4-fold decrease in the rate of heme b_H reduction (26). Similar levels of decrease in V_{max} with E295V compared to the wild-type were observed in the present work (Table 1). The kinetic data thus confirmed that the E295V substitution did not alter significantly the binding affinity of QH_2 molecules at the Q_o site of cyt bc_1, but it rather decreased conspicuously the catalytic efficiency (V_{max}/K_m) of the enzyme during Q_o catalysis. This result implies that substitution of E295 perturbs the Q_o site, generating a rate-limiting step in either electron or proton transfers. The observation that yeast E272V or bacterial E295V mutants did not show any significant effect on the Q_i site-mediated reverse electron transfer rate (37) or the Q_o site-mediated cyt b_H reduction rates (26), respectively, suggests that no alteration of the electron transfer pathway is caused by the E295V mutation. In addition, the physicochemical properties of cyt bc_1 (*i.e.*, $E_{m,7}$ of hemes b_L and b_H or redox sensitive spectra) were not altered by mutation of E295 in bacterial cyt bc_1 (26, 38). On the other hand, the rate of b_H reduction of E295Q at different pH values in bacterial (26), as well as the turnover rate of cyt *c* reduction in E272D and Q at below pH 6 in yeast (36) mutants were significantly decreased as compared to those of the corresponding wild-type enzymes. These findings pointed out that the observed catalytic defect might be linked to the

proton-active carboxylate group of E295, although this effect was not seen with the yeast E272P and E272V mutants (37).

Zn^{2+} inhibition kinetics of cyt bc_1

Previous EXAFS spectroscopy of Zn^{2+} stoichiometrically bound to cyt bc_1 (24), together with several other studies (17, 26, 36–39), suggested that steps of protonation and deprotonation of E295 are closely linked to the rate-limiting Q_o site proton exchange. Zn^{2+} binding assay using eukaryotic cyt bc_1 suggested that this enzyme has multiple independent Zn^{2+} binding sites with different affinities (39). From the binding assay with radio labeled Zn^{2+}, bovine cyt bc_1 was found to have two types of binding sites with different stoichiometry and affinity at pH 7.2; a high affinity site (n, 1.1 ± 0.1 Zn^{2+}/c_1; K_I, 0.13 μM) and several low affinity sites (n, 3 – 4 Zn^{2+}/c_1; K_I, 2.3 μM) (39). The chicken cyt bc_1 has a higher K_I (3 μM) with respect to the bovine enzyme, and crystallographic studies initially indicated two different Zn^{2+} binding sites (25). However, subsequent analyses revealed that it has only one site (see the PDB structure 3h1k, remark 280). Accordingly, Zn^{2+}-inhibitory kinetics studies were performed with purified bacterial wild type and E295V mutant enzymes at various concentrations of Zn^{2+}. Simple inhibition curves were obtained when purified *R. capsulatus* cyt bc_1 was titrated with Zn^{2+} in 40 mM Tris-HCl buffer (Fig. 2). The inhibition curves were fitted by a standard inhibition equation assuming either one or two independent types of inhibition site(s). The K_I could be obtained by fitting the Zn^{2+} dependence with a single homogeneous inhibition site: $v = V_{max}/(1 + [Zn^{2+}]/K_I)$ (Eq. 1). At $[Zn^{2+}] > 0.2$ mM, only 10% of original activity remained (Fig. 2), but there was no additional decrease of activity up to 0.6 mM Zn^{2+}. In 40 mM Tris-HCl buffer at pH 7.5, wild-type cyt bc_1 showed a K_I value of 0.9×10^{-6} M for Zn^{2+}, which is lower than that of the chicken cyt bc_1 (25). On the other hand, E295V exhibited a K_I value of 2.6×10^{-6} M, which is approximately 3-fold higher than that of the wild type (Fig. 2 and Table 2). In addition, some residual activity (30%) of E295V was observed even at $[Zn^{2+}] > 0.2$ mM. The Zn^{2+} binding affinities of wild type and mutant cyt bc_1 derivative were determined more directly using microcalorimetry.

Cyt bc_1 Zn^{2+} binding properties studied by isothermal titration calorimetry

ITC measurements were carried out with the goal of (i) detecting, using an independent approach, the presence of a high affinity Zn^{2+} binding site in the wild-type cyt bc_1, (ii) determining the dissociation constant K_D of the Zn^{2+} complex and (iii) comparing the binding properties of the wild-type cyt bc_1 with those of the E295V mutant derivative. The ITC measurements were performed by adding Zn^{2+} to the cyt bc_1 suspensions in the Tris-HCl pH 7.5 buffer. The occurrence of binding events was revealed by the presence of exothermic peaks that followed each Zn^{2+} addition as shown in Fig. 3A. The titrations obtained from the integrated heat data for the wild-type and E295V mutant cyt bc_1 enzymes are compared in Fig. 3B. Titrations were fitted to two different models characterized either by a single set or by two sets of independent, non-interacting binding sites. Each set had a number n of binding sites per protein complex, possessing the same intrinsic dissociation constant K_D. Both in the wild-type and in the E295V mutant enzymes the inclusion of a second binding event improved significantly the quality of the fit. When the data was fitted by using the two-site model equation, the wild-type cyt bc_1 (Fig. 3B, black circles) had two K_D values of 0.5×10^{-6} M (K_{D1} = 0.50 ± 0.07 μM) and 6.8×10^{-6} M (K_{D2} = 6.8 ± 0.9 μM) with a stoichiometry n_1 = 1.13 ± 0.03 for the high affinity site, and n_2 = 3.7 ± 0.2 for a few lower affinity binding sites, respectively (Fig. 3B and Table 2). The two binding events are driven by favorable enthalpic factors, $\Delta H_1 = -5.6 \pm 0.2$ kcal/mol and $\Delta H_2 = -1.4 \pm 0.2$ kcal/mol, respectively. A second independent set of data (not shown) acquired for the wild-type enzyme at a comparable concentration of total protein yielded a titration essentially coincident with that shown in Fig. 3B, indicating that the results were highly reproducible. It

has been noted that the K_D of the high affinity Zn^{2+} binding site of the bovine cyt bc_1 was essentially identical to the inhibition constant K_I under all conditions tested (39). A similar situation is found here for the bacterial cyt bc_1. Zn^{2+} binds stoichiometrically to a high affinity cyt bc_1 site, and characterized by a dissociation constant, K_D (0.5×10^{-6} M) that has the same order-of-magnitude of the K_I (0.9×10^{-6} M) determined by measuring the inhibition kinetics of Zn^{2+} under similar conditions (Fig. 2). Therefore, we infer that binding of Zn^{2+} to the high affinity site of cyt bc_1 caused its inhibition, whereas the additional low affinity binding sites did not seem to induce additional inhibition of the catalytic activity. The presence of a few low affinity-binding sites was also detected in eukaryotic cyt bc_1 (39).

A quite distinct binding ITC pattern was observed in the E295V mutant, for which the titration (Fig. 3B, open circles) suggested that saturation of Zn^{2+} binding is attained at higher metal/protein ratios. Again, as observed in the wild type complex, the one-site model was unable to describe adequately the titration, revealing the presence of additional binding sites. A blind fit to the data according to the two-site model, in which the free parameters of the fit were the number of binding sites n_i, the enthalpy change ΔH_i and the dissociation constant K_{Di} (for each set i of binding sites), yielded $n_1 = 1.97 \pm 0.08$ and $K_D = 0.55 \pm 0.09$ μM for the higher affinity set, with $\Delta H_1 = -9.9 \pm 0.7$ kcal/mol, plus a number $n_2 = 7.1 \pm 0.3$ of low affinity binding sites per cyt bc_1, characterized by $K_{D2} = 5.81 \pm 1.22$ μM and $\Delta H_2 = -2.6 \pm 0.3$ kcal/mol. However an equivalently good fit to the data, as judged from the essentially unaffected chi-square value, could be obtained by reducing the number of free parameters, *i.e*. by fixing the stoichiometry of a set of binding sites to a unitary value, as found in the case of wild type cyt bc_1 for the high affinity site. This choice resulted in a stoichiometric high affinity binding site characterized by $K_{D1} = 1.0 \times 10^{-6}$ M (1.00 ± 0.36 μM) and an enthalpy change $\Delta H_1 = -28 \pm 4$ kcal/mol, in addition to a number $n_2 = 9.1 \pm 0.5$ of low affinity sites characterized by $K_{D2} = 3.5 \times 10^{-6}$ M (3.5 ± 1.6 μM) and $\Delta H_2 = -0.9 \pm 0.5$ kcal/mol. Although the two fits are essentially equivalent on a purely statistical basis, the physical interpretation of the latter fit is simpler, since it appears rather unlikely that the substitution of E295 leads to the high affinity binding of two Zn^{2+} ions in the same binding pocket or in its vicinity. The physically meaningful assumption of a unitary stoichiometry for a set of binding sites results in the increase by a factor of two in the dissociation constant K_{D1} of the high affinity Zn^{2+} binding site in the E295V as compared to the wild type. Such an effect is consistent with a comparable increase in the value of the inhibitory constant K_I, as evaluated from the Zn^{2+} inhibition kinetics (Fig. 2). Together with the inhibition kinetics, the ITC analysis thus indicated that substitution of E295 weakens the Zn^{2+} binding to the Q_o site of the cyt bc_1, supporting the notion that E295 belongs to the metal ligand cluster (24).

The dissociation constants and thermodynamic parameters provided in the present study do not take into account possible events of proton transfer linked to metal binding, or the presence in solution of complexes between the metal ions and the buffer. This treatment is beyond the scope of the present study. However, the values of the measured equilibrium constants compare well with those reported in the literature and determined using ITC or other methodologies, which, in principle, should also take into account similar effects. These values are therefore only used for comparison purposes of native and mutant cyt bc_1 enzymes.

Redox-induced FTIR difference spectroscopy

To investigate further whether Zn^{2+} inhibition occurs via E295 at the Q_o site of the cyt bc_1, we performed the redox-induced FTIR difference spectra analyses using wild-type cyt bc_1, its E295V mutant, as well as a cyt b-c_1 subcomplex lacking the Fe/S protein (28), in the presence and absence of Zn^{2+} (Fig. 4). The redox-induced FTIR difference spectra provide information on the protonation state of acidic residues or quinone binding, as described previously (35, 38, 40, 41). The positive and negative signals in the spectra correlate with

the oxidized, and the reduced forms of the enzyme, respectively. Figure 4 shows an overview of the oxidized *minus* reduced FTIR difference spectra of the wild-type cyt bc_1, E295V mutant and the cyt b-c_1 subcomplex lacking the Fe/S protein. The spectra are dominated by signals from the free and bound quinones, and include the amide-I and amide-II bands as well as signals from individual amino acids. Purified wild-type cyt bc_1 with and without Zn^{2+} retained their bound quinones as judged by their intense signals observed at 1288 and 1263 cm^{-1}, ascribed to the methoxy side chain (the C-O modes) of quinones. Alternatively, the signal at 1263 cm^{-1} may also be contributed indirectly by heme b_H or by cyt c_1 $\delta(C_m–H)$ vibration. The spectral region between 1750 and 1700 cm^{-1} includes information about the protonated Asp/Glu residues, and can be used as a good indicator of the environment of these redox active amino acids. The oxidation-induced protonation of acidic residues gives rise to a positive signal at 1739 cm^{-1}, which was previously assigned to the υ(C=O) vibration of D278 and E295 residues in cyt bc_1 (26, 35, 36, 38, 41). The negative signal observed at 1720 cm^{-1} can be assigned to the υ(C=O) vibration of protonated acidic residues. The presence of a pair of signals (+) 1739 cm^{-1} and (−) 1720 cm^{-1} is typical of the modification of the environment of redox active acidic residues upon redox reaction (42). In fact, the higher the frequency is, the more hydrophobic the environment of the acidic residue is. The downshift of the negative signal indicates that the acidic residue is involved in stronger H-bonds, or is more exposed to the solvent in the reduced form. This behavior points toward a conformational change of the residue upon redox reaction. A positive signal can be seen at 1706 cm^{-1}. This signal was tentatively assigned to an acidic residue located in the heme *b* subunit of *P. denitrificans* (38, 43). Furthermore, this signal can arise also from the υ(C=O) vibration of the heme propionates. Upon addition of Zn^{2+}, this signal decreased in intensity. In addition, the positive mode at 1739 cm^{-1} shifts to 1745 cm^{-1}, indicating that protonated Asp/Glu residues form stronger H-bonds upon reduction. Clearly, the FTIR spectra of the wild-type cyt bc_1 showed a direct interaction between acidic residue(s) and Zn^{2+}.

Compared to the FTIR difference spectrum of the wild-type the spectrum of the E295V mutant showed weaker signals in the spectral region for the protonated acidic residues, indicating that the E295 residue is responsible for the signals observed at 1739 and 1720 cm^{-1} in the difference spectrum of the wild-type. On the other hand, addition of Zn^{2+} to E295V did not show any redox dependent signal as seen in the spectrum of the wild-type, suggesting that the E295 residue is a direct Zn^{2+} ligand as well as representing a proton exit group in cyt bc_1. The redox-dependent secondary structure modifications can be seen in the region of the amide I band (44). The most prominent signal observed at 1650 cm^{-1}, assigned to the υ(C=O) vibrational mode of neutral fully oxidized quinones, was slightly altered by Zn^{2+} binding in the wild-type spectra, and in that for the E295V mutant enzyme the signal was found to be slightly shifted and having a larger half-with (Fig. 4). The signals from the deprotonated heme propionates are expected in the so-called amide-II region from 1560-1500 cm^{-1}, but they overlap with the side chain contribution of deprotonated acidic residues (41, 43). Note that these contributions could be seen as negative signals in the difference spectra at 1560 and 1536 cm^{-1} for the wild-type cyt bc_1. The positive signal at 1547 cm^{-1} can be assigned to amide II vibration as well as to the υ_{38} vibration of heme b_L. Upon Zn^{2+} inhibition, a positive signal appears in the difference spectrum at 1571 cm^{-1} which can be assigned to the $\upsilon(COO^-)^{as}$ vibration of deprotonated acidic residues. This signal could arise from the acidic residues that bind Zn^{2+}. This observation leads to the conclusion that the relevant acidic residue binds Zn^{2+} via its carboxyl moiety.

H-D exchange leads to an uncoupling and downshift of the amide-II band to about 1450 cm^{-1}, thus clarifying the signature of the deprotonated acidic residues as well as the heme propionates. The difference spectra of the wild-type and Zn^{2+}-inhibited cyt bc_1 recorded at pD 8.0 are presented in Fig. 5. These spectra show that the signal observed at 1536 cm^{-1} in

the difference spectrum of the wild-type is absent after H-D exchange. Indeed, this signal arises from the amide-II modes, downshifted upon H-D exchange. Another major spectral change was observed at ≤ 1400 cm^{-1}, at 1390, 1384 and 1362 cm^{-1} in the wild type. These signals include the coordinates from the quinones ring motions, $\upsilon(COO^{-})^{s}$ of Asp/Glu (heme b_H) or the heme propionate. When Zn^{2+} was bound to cyt bc_1, only two signals at 1407 and 1388 cm^{-1} remain visible in the spectrum. However, in the spectrum of the E295V mutant enzyme no signal was evident in this spectral region, indicating that there was no effect of Zn^{2+} binding on the E295 residue and the hemes.

The specific porphyrin ring motions can be observed between 1000 and 800 cm^{-1} and are sensitive to pH (34, 45, 46). The difference spectrum of the wild type contains a negative signal at 964 cm^{-1}, and a positive signal at 930 cm^{-1}, assigned to the ring deformation vibration of the imidazole (47, 48). It is thus likely that the coordinating His of the heme groups gives rise to these signals. Upon addition of Zn^{2+}, these signals lose intensity, suggesting that the relevant His residue(s) is (are) not perturbed by the reaction anymore. The redox sensitive signal appearing at 835 cm^{-1} is shifted towards 827 cm^{-1} upon reduction. This signal was previously assigned to the $\gamma(C_m\text{-}H)$ vibration of the porphyrin ring (34). The frequency of the $\gamma(C_m\text{-}H)$ vibration depends also on the pH. At high pH, the 835 cm^{-1} signal is found at high frequency, and at low pH, it is found at low frequency (*i.e.* 827 cm^{-1}). This behavior indicates that the heme propionates are in the protonated state in the oxidized form and deprotonated in the reduced state. The inhibition induces the splitting of the negative signal into two signals at 825 and 815 cm^{-1}. Thus, the addition of Zn^{2+} modifies the protonation state of the propionates and/or the His that coordinate the iron of the hemes. The heme signature of the E295V mutant is similar to that observed for the inhibited wild-type, indicating that this mutation has a similar effect as the inhibition on the protonation state of the hemes.

UV/Vis difference spectroscopy and titration of cyt bc_1 hemes

The UV/Vis redox difference spectra of the wild-type, the E295V mutant and the cyt *b*-c_1 subcomplex lacking the Fe/S protein were compared in the presence and absence of Zn^{2+} with respect to the γ-band at 428 nm and α-band at 524, 552 and 558 nm (Fig. 6A). All enzymes were fully oxidized in 5 minutes at +500 mV vs SHE and fully reduced within 7 minutes at −500 mV vs SHE, indicating that either mutating E295 or absence of the Fe/S protein does not affect the redox behavior of the hemes *b* and c_1 of cyt bc_1 (Fig. 6A). On the other hand, addition of Zn^{2+} slowed down the reduction behavior observed as the fully reduced samples were obtained in 10 minutes after the application of the reducing potential (data not shown) while the oxidation rate remained unaffected.

UV/Vis titrations were performed by monitoring the absorbance of the Soret band of the wild-type enzyme in the presence and absence of Zn^{2+} to determine the effect of Zn^{2+} binding on the midpoint potentials of the hemes of cyt bc_1 (Fig. 6B and 6C). The oxidative titration curves showed that Zn^{2+} inhibition does not significantly affect the midpoint potentials of the *b*-type hemes, whereas the midpoint potential of E295V mutant heme c_1 seemed to be slightly shifted in the presence of Zn^{2+}. However, we note that the equilibration time is typically very long for the heme c_1 leading to a higher error than seen for the other hemes.

Discussion

The vectorial proton translocation across the membrane for the generation of ΔpH involves cyt bc_1, whose proton-transfer pathways are not well defined. The E295 residue found in the highly conserved PEWY motif of the cyt *b* subunit of cyt bc_1 might play an important role in the release of protons when QH_2 oxidation occurs. Clearly, mutation in this residue affects

the electron transferring activity of cyt bc_1 as shown in several studies with bovine, yeast and bacterial cyt bc_1 (17, 26, 36, 37). Nevertheless, its role in either Q/QH_2 binding for the formation of enzyme-substrate (ES) complex (17, 36) or in proton release associated with H_2O molecules near the Q_o site (26, 37, 38) remained less clear. Considering these possibilities, here we performed Zn^{2+} inhibition studies using steady-state kinetics, ITC analysis and redox-induced difference FTIR spectroscopy with both the native and the E295V mutant derivative of cyt bc_1.

The kinetic parameters for cyt bc_1 were obtained as a first approximation using a simple Michaelis-Menten kinetics with DBH_2 as a substrate to compare the E295V mutant with the wild type enzyme under steady-state conditions (Table 1). E295V has a 4-fold lower V_{max} value than the wild type, whereas its K_m value for DBH_2 was only marginally lower. Thus, its lower V_{max} affected its apparent catalytic efficiency V_{max}/K_m. Previously, E295 was proposed to be an important residue to form an ES complex at the Q_o site through formation of a H-bond with the OH group of stigmatellin that might mimic a reaction intermediate (*i.e.*, either SQ or QH_2) based on the crystal structures of cyt bc_1 (17, 36). However, substitution of E295 with various amino acids revealed robustness of the cyt bc_1 electron transferring activity (26), suggesting that this residue may not be involved in substrate binding to form the ES complex, but might rather influence later steps of proton transfer directly or indirectly (37). This suggestion was confirmed by our kinetic data (Table 1). Indeed, addition of Zn^{2+} in the μmolar range severely inhibited the wild-type cyt bc_1, whereas E295V, featuring a 4-fold higher K_I value than the wild type, was less sensitive to Zn^{2+} (Fig. 2). These kinetic results, pointing to a role of E295 in the inhibitory binding of Zn^{2+}, are consistent with cyt bc_1 metal binding properties determined by ITC (Fig. 3). Indeed, in the wild type cyt bc_1 ITC analysis showed the presence of a high affinity Zn^{2+} binding site, characterized by a dissociation constant K_D of the same order-of-magnitude of the inhibitory constant K_I derived from the kinetic study under similar conditions. Interestingly, a similar matching between the K_D of the high affinity Zn^{2+} binding site and the inhibition constant K_I has been previously observed for the bovine cyt bc_1, using a different approach to determine the binding parameters, under the conditions tested (39). As observed in the eukaryotic cyt bc_1 (39), in the case of bacterial cyt bc_1 the ITC analysis revealed additional Zn^{2+} binding sites that are characterized by a dissociation constant ten times higher than that of the inhibitory high affinity site. These sites are likely to reflect less specific interactions with the metal ion, and are unrelated to Zn^{2+} inhibition of the catalytic activity. Furthermore, analysis of the data of the titration effected with the E295V mutant indicates that the Zn^{2+} binding is weakened as compared to the wild-type, paralleling the weaker inhibition observed in the kinetic studies. Consequently, both kinetic and ITC data support the previous proposal based on EXAFS analysis (24) that E295 is one of the Zn^{2+} ligands, further suggesting that the E295 residue as the Zn^{2+} ligand is involved in the proton release of cyt bc_1.

We further investigated the involvement of residue E295 in Zn^{2+} binding using both redox-induced FTIR difference, and UV-visible redox difference, spectra of the wild-type and E295V mutant complex in the absence and presence of Zn^{2+}, as well as we determined the mid-point potentials of hemes *b* and *c* cofactors of cyt bc_1 (Fig. 6). The electron transfer rate reflected by the redox behavior of cyts *b* and *c* showed that Zn^{2+} slowed down the electron transfer activity of the cyt bc_1. This was also supported by the observation that the typical infrared signature (below 1000 cm^{-1}) of the porphyrin ring of the Zn^{2+} bound wild-type enzyme was similar to that of E295V without Zn^{2+}, indicating that E295 might contribute to provide favorable conformational changes for the occurrence of bifurcated electron transfer at the Q_o site. However, loss of such changes, due to the presence of Zn^{2+} or the E to V substitution, did not alter the redox potentials of hemes *b* and c_1 cofactors even in the presence of Zn^{2+} (Fig. 6B and C). Thus, these data indicated that neither substrate binding

(K_m) nor ES complex formation (lower E_a) requires E295 necessarily (17). Rather, as previously suggested (26, 37), upon binding and oxidation of QH_2 at the Q_o site, this residue seems to contribute to forming a pathway associated with H_2O for proton release during the Q_o catalysis. Regardless of the presence and absence of Zn^{2+}, substitution of E295 diminished the signals of protonated acidic residue in both oxidized and reduced forms (at 1746 cm^{-1} and 1722 cm^{-1}, respectively) as well as the signals of deprotonated residues in the reduced form, typically observed in the wild type. On the other hand, the wild-type enzyme inhibited by Zn^{2+} also lost these signals, indicating that Zn^{2+} interfered directly with protonation/deprotonation of E295 in cyt bc_1. In addition, Zn^{2+} could bind the E295 residue directly via carboxylate moiety as observed from the $\upsilon(COO^-)$ vibrational mode at 1560 cm^{-1} (Fig. 4). Earlier FTIR studies showed that in *Paracoccus denitrificans* cyt bc_1 bound to stigmatellin, E295 is H-bonded to the carbonyl group of this inhibitor in the oxidized form (38). The FTIR spectroscopic data strongly suggested that protonation/deprotonation of E295 might be important for displacement of its carboxylate side chain at the Q_o site, resulting in the modification of the relative hydrophobicity of the Q_o cavity facing the outer membranes surface, which is highly associated with H_2O molecules. Consequently, it appears that a perturbed protonation/deprotonation state of E295, by either mutation or Zn^{2+} binding, prevents a facilitated movement of the side chain of this residue towards the propionate group of heme b_L. This would hamper the rapid release of a proton from the Q_o site, resulting in slower electron transfer to the low potential chain.

Notably, the removal of the Fe/S protein from the cyt bc_1 induced inaccessibility of Zn^{2+} to E295 (Fig. 4). Although the Fe/S protein is not likely to participate in Zn^{2+} binding directly, it is possible that a conformational change in the *ef* loop, due to absence of the Fe/S protein, might drastically modify the location of the PEWY motif, resulting in the displacement of E295 toward the more hydrophobic inner portion of the membrane, hampering Zn^{2+} accessibility. Other cyt *b* residues such as H276, D278 and N279 that ligand Zn^{2+} were additionally proposed to act as proton exit paths on the basis of EXAFS studies (24). Recent FTIR data with D278 in *P. denitrificans* cyt bc_1 indicated that even in the presence of stigmatellin, this residue remains protonated in the oxidized form, but its vibrational frequency shifts in the reduced form (38). Therefore, it will be worthy to investigate further the role of these residues on proton pathways of cyt bc_1 using site-directed mutagenesis coupled to an analogous experimental approach as described in the present work. These studies are underway in our laboratories.

Abbreviations

Cyt	cytochrome
cyt bc_1	ubihydroquinone:cyt *c* oxidoreductase
Fe/S	iron sulfur
Q_o	hydroquinone oxidation
Q_i	quinone reduction
QH_2	hydroquinone
Q	quinone
SQ	semiquinone
MPYE	mineral-peptone-yeast-extract
MOPS	4-morpholinepropanesulfonic acid
DBH_2	decylbenzohydroquinone

DDM	dodecyl maltoside
EPR	electron paramagnetic resonance
ITC	isothermal titration calorimetry
FTIR	Fourier transform infrared

References

1. Papa S, Lorusso M, Di Paola M. Cooperativity and flexibility of the protonmotive activity of mitochondrial respiratory chain. Biochim Biophys Acta. 2006; 1757:428–436. [PubMed: 16730640]
2. Trumpower BL. The protonmotive Q cycle. Energy transduction by coupling of proton translocation to electron transfer by the cytochrome bc_1 complex. J Biol Chem. 1990; 265:11409–11412. [PubMed: 2164001]
3. Berry EA, Guergova-Kuras M, Huang LS, Crofts AR. Structure and function of cytochrome *bc* complexes. Annu Rev Biochem. 2000; 69:1005–1075. [PubMed: 10966481]
4. Darrouzet E, Cooley JW, Daldal F. The cytochrome bc_1 complex and its homologue the b_6f complex: similarities and differences. Photosynth Res. 2004; 79:25–44. [PubMed: 16228398]
5. Iwata S, Lee JW, Okada K, Lee JK, Iwata M, Rasmussen B, Link TA, Ramaswamy S, Jap BK. Complete structure of the 11-subunit bovine mitochondrial cytochrome bc_1 complex. Science. 1998; 281:64–71. [PubMed: 9651245]
6. Darrouzet E, Moser CC, Dutton PL, Daldal F. Large scale domain movement in cytochrome bc_1: a new device for electron transfer in proteins. Trends Biochem Sci. 2001; 26:445–451. [PubMed: 11440857]
7. Zhang Z, Huang L, Shulmeister VM, Chi YI, Kim KK, Hung LW, Crofts AR, Berry EA, Kim SH. Electron transfer by domain movement in cytochrome bc_1. Nature. 1998; 392:677–684. [PubMed: 9565029]
8. Xia D, Yu CA, Kim H, Xia JZ, Kachurin AM, Zhang L, Yu L, Deisenhofer J. Crystal structure of the cytochrome bc_1 complex from bovine heart mitochondria. Science. 1997; 277:60–66. [PubMed: 9204897]
9. Jenney FE Jr, Prince RC, Daldal F. The membrane-bound cytochrome c_y of *Rhodobacter capsulatus* can serve as an electron donor to the photosynthetic reaction of *Rhodobacter sphaeroides*. Biochim Biophys Acta. 1996; 1273:159–164. [PubMed: 8611589]
10. Jenney FE Jr, Prince RC, Daldal F. Roles of the soluble cytochrome c_2 and membrane-associated cytochrome c_y of *Rhodobacter capsulatus* in photosynthetic electron transfer. Biochemistry. 1994; 33:2496–2502. [PubMed: 8117711]
11. Jenney FE Jr, Daldal F. A novel membrane-associated *c*-type cytochrome, cyt c_y, can mediate the photosynthetic growth of *Rhodobacter capsulatus* and *Rhodobacter sphaeroides*. EMBO J. 1993; 12:1283–1292. [PubMed: 8385603]
12. Gray KA, Dutton PL, Daldal F. Requirement of histidine 217 for ubiquinone reductase activity (Q_i site) in the cytochrome bc_1 complex. Biochemistry. 1994; 33:723–733. [PubMed: 8292600]
13. Wang Y, Obungu V, Beattie DS. Dicyclohexylcarbodiimide inhibits proton pumping in ubiquinol:cytochrome *c* oxidoreductase of *Rhodobacter sphaeroides* and binds to aspartate-187 of cytochrome *b*. Arch Biochem Biophys. 1998; 352:193–198. [PubMed: 9587406]
14. Shinkarev VP, Ugulava NB, Crofts AR, Wraight CA. DCCD inhibits the reactions of the iron-sulfur protein in *Rhodobacter sphaeroides* chromatophores. Biochemistry. 2000; 39:16206–16212. [PubMed: 11123950]
15. Shinkarev VP, Ugulava NB, Takahashi E, Crofts AR, Wraight CA. Aspartate-187 of cytochrome *b* is not needed for DCCD inhibition of ubiquinol: cytochrome *c* oxidoreductase in *Rhodobacter sphaeroides* chromatophores. Biochemistry. 2000; 39:14232–14237. [PubMed: 11087372]
16. Wang Y, Beattie DS. Molecular modeling studies of the DCCD-treated cytochrome bc_1 complex: predicted conformational changes and inhibition of proton translocation. J Bioenerg Biomembr. 2002; 34:81–88. [PubMed: 12018891]

17. Crofts AR, Hong S, Ugulava N, Barquera B, Gennis R, Guergova-Kuras M, Berry EA. Pathways for proton release during ubihydroquinone oxidation by the bc_1 complex. Proc Natl Acad Sci U S A. 1999; 96:10021–10026. [PubMed: 10468555]
18. Utschig LM, Ohigashi Y, Thurnauer MC, Tiede DM. A new metal-binding site in photosynthetic bacterial reaction centers that modulates Q_A to Q_B electron transfer. Biochemistry. 1998; 37:8278–8281. [PubMed: 9622479]
19. Giachini L, Francia F, Mallardi A, Palazzo G, Carpene E, Boscherini F, Venturoli G. Multiple scattering X-ray absorption studies of Zn^{2+} binding sites in bacterial photosynthetic reaction centers. Biophys J. 2005; 88:2038–2046. [PubMed: 15613631]
20. Adelroth P, Paddock ML, Sagle LB, Feher G, Okamura MY. Identification of the proton pathway in bacterial reaction centers: both protons associated with reduction of Q_B to Q_BH_2 share a common entry point. Proc Natl Acad Sci U S A. 2000; 97:13086–13091. [PubMed: 11078513]
21. Axelrod HL, Abresch EC, Paddock ML, Okamura MY, Feher G. Determination of the binding sites of the proton transfer inhibitors Cd^{2+} and Zn^{2+} in bacterial reaction centers. Proc Natl Acad Sci U S A. 2000; 97:1542–1547. [PubMed: 10677497]
22. Qin L, Mills DA, Hiser C, Murphree A, Garavito RM, Ferguson-Miller S, Hosler J. Crystallographic location and mutational analysis of Zn and Cd inhibitory sites and role of lipidic carboxylates in rescuing proton path mutants in cytochrome *c* oxidase. Biochemistry. 2007; 46:6239–6248. [PubMed: 17477548]
23. Mills DA, Schmidt B, Hiser C, Westley E, Ferguson-Miller S. Membrane potential-controlled inhibition of cytochrome *c* oxidase by zinc. J Biol Chem. 2002; 277:14894–14901. [PubMed: 11832490]
24. Giachini L, Francia F, Veronesi G, Lee DW, Daldal F, Huang LS, Berry EA, Cocco T, Papa S, Boscherini F, Venturoli G. X-Ray absorption studies of Zn^{2+} binding sites in bacterial, avian, and bovine cytochrome bc_1 complexes. Biophys J. 2007; 93:2934–2951. [PubMed: 17573435]
25. Berry EA, Zhang Z, Bellamy HD, Huang L. Crystallographic location of two Zn^{2+}-binding sites in the avian cytochrome bc_1 complex. Biochim Biophys Acta. 2000; 1459:440–448. [PubMed: 11004461]
26. Osyczka A, Zhang H, Mathe C, Rich PR, Moser CC, Dutton PL. Role of the PEWY glutamate in hydroquinone-quinone oxidation-reduction catalysis in the Q_o Site of cytochrome bc_1. Biochemistry. 2006; 45:10492–10503. [PubMed: 16939201]
27. Atta-Asafo-Adjei E, Daldal F. Size of the amino acid side chain at position 158 of cytochrome *b* is critical for an active cytochrome bc_1 complex and for photosynthetic growth of *Rhodobacter capsulatus*. Proc Natl Acad Sci U S A. 1991; 88:492–496. [PubMed: 1846443]
28. Valkova-Valchanova MB, Saribas AS, Gibney BR, Dutton PL, Daldal F. Isolation and characterization of a two-subunit cytochrome b-c_1 subcomplex from Rhodobacter capsulatus and reconstitution of its ubihydroquinone oxidation (Q_o) site with purified Fe-S protein subunit. Biochemistry. 1998; 37:16242–16251. [PubMed: 9819216]
29. Lee DW, Ozturk Y, Osyczka A, Cooley JW, Daldal F. Cytochrome bc_1-c_y fusion complexes reveal the distance constraints for functional electron transfer between photosynthesis components. J Biol Chem. 2008; 283:13973–13982. [PubMed: 18343816]
30. Smith PK, Krohn RI, Hermanson GT, Mallia AK, Gartner FH, Provenzano MD, Fujimoto EK, Goeke NM, Olson BJ, Klenk DC. Measurement of protein using bicinchoninic acid. Anal Biochem. 1985; 150:76–85. [PubMed: 3843705]
31. Laemmli UK. Cleavage of structural proteins during the assembly of the head of bacteriophage T4. Nature. 1970; 227:680–685. [PubMed: 5432063]
32. Rich PR. Electron and proton transfers through quinones and cytochrome *bc* complexes. Biochim Biophys Acta. 1984; 768:53–79. [PubMed: 6322844]
33. Moss D, Nabedryk E, Breton J, Mantele W. Redox-linked conformational changes in proteins detected by a combination of infrared spectroscopy and protein electrochemistry. Evaluation of the technique with cytochrome *c*. Eur J Biochem. 1990; 187:565–572. [PubMed: 2154376]
34. Dorr S, Wolpert M, Hellwig P. Study on the redox state dependent gamma(CH) vibrational modes of the *c*-type heme. Biopolymers. 2006; 82:349–352. [PubMed: 16419062]

35. Ritter M, Palsdottir H, Abe M, Mantele W, Hunte C, Miyoshi H, Hellwig P. Direct evidence for the interaction of stigmatellin with a protonated acidic group in the bc_1 complex from *Saccharomyces cerevisiae* as monitored by FTIR difference spectroscopy and 13C specific labeling. Biochemistry. 2004; 43:8439–8446. [PubMed: 15222755]
36. Wenz T, Hellwig P, MacMillan F, Meunier B, Hunte C. Probing the role of E272 in quinol oxidation of mitochondrial complex III. Biochemistry. 2006; 45:9042–9052. [PubMed: 16866349]
37. Seddiki N, Meunier B, Lemesle-Meunier D, Brasseur G. Is cytochrome *b* glutamic acid 272 a quinol binding residue in the bc_1 complex of *Saccharomyces cerevisiae*? Biochemistry. 2008; 47:2357–2368. [PubMed: 18215069]
38. Kleinschroth T, Anderka O, Ritter M, Stocker A, Link TA, Ludwig B, Hellwig P. Characterization of mutations in crucial residues around the Q_o binding site of the cytochrome *bc* complex from *Paracoccus denitrificans*. FEBS J. 2008; 275:4773–4785. [PubMed: 18721136]
39. Link TA, von Jagow G. Zinc ions inhibit the Q_P center of bovine heart mitochondrial bc_1 complex by blocking a protonatable group. J Biol Chem. 1995; 270:25001–25006. [PubMed: 7559629]
40. Iwaki M, Giotta L, Akinsiku AO, Schagger H, Fisher N, Breton J, Rich PR. Redox-induced transitions in bovine cytochrome bc_1 complex studied by perfusion-induced ATR-FTIR spectroscopy. Biochemistry. 2003; 42:11109–11119. [PubMed: 14503861]
41. Baymann F, Robertson DE, Dutton PL, Mantele W. Electrochemical and spectroscopic investigations of the cytochrome bc_1 complex from *Rhodobacter capsulatus*. Biochemistry. 1999; 38:13188–13199. [PubMed: 10529191]
42. Hellwig P, Behr J, Ostermeier C, Richter OM, Pfitzner U, Odenwald A, Ludwig B, Michel H, Mantele W. Involvement of glutamic acid 278 in the redox reaction of the cytochrome *c* oxidase from *Paracoccus denitrificans* investigated by FTIR spectroscopy. Biochemistry. 1998; 37:7390–7399. [PubMed: 9585553]
43. Ritter M, Anderka O, Ludwig B, Mantele W, Hellwig P. Electrochemical and FTIR spectroscopic characterization of the cytochrome bc_1 complex from *Paracoccus denitrificans*: evidence for protonation reactions coupled to quinone binding. Biochemistry. 2003; 42:12391–12399. [PubMed: 14567700]
44. Kong J, Yu S. Fourier transform infrared spectroscopic analysis of protein secondary structures. Acta Biochim Biophys Sin (Shanghai). 2007; 39:549–559. [PubMed: 17687489]
45. Dorr S, Schade U, Hellwig P. Far infrared spectroscopy on hemoproteins: A model compound study from 1800-100 cm^{-1}. Vib Spectrosc. 2008; 47:59–65.
46. Berthomieu C, Marboutin L, Dupeyrat F, Bouyer P. Electrochemically induced FTIR difference spectroscopy in the mid- to far infrared (200 μm) domain: a new setup for the analysis of metal-ligand interactions in redox proteins. Biopolymers. 2006; 82:363–367. [PubMed: 16453337]
47. Hasegawa K, Ono T, Noguchi T. Vibrational spectra and ab initio DFT calculations of 4-methylimidazole and its different protonation forms: Infrared and raman markers of the protonation state of a histidine side chain. J Phys Chem B. 2000; 104:4253–4265.
48. Wolpert M, Hellwig P. Infrared spectra and molar absorption coefficients of the 20 alpha amino acids in aqueous solutions in the spectral range from 1800 to 500 cm^{-1}. Spectrochim Acta A Mol Biomol Spectrosc. 2006; 64:987–1001. [PubMed: 16458063]
49. Berry EA, Huang LS, Saechao LK, Pon NG, Valkova-Valchanova M, Daldal F. X-ray structure of *Rhodobacter capsulatus* cytochrome bc_1: comparison with its mitochondrial and chloroplast counterparts. Photosynth Res. 2004; 81:251–275. [PubMed: 16034531]
50. Gazaryan IG, Krasnikov BF, Ashby GA, Thorneley RN, Kristal BS, Brown AM. Zinc is a potent inhibitor of thiol oxidoreductase activity and stimulates reactive oxygen species production by lipoamide dehydrogenase. J Biol Chem. 2002; 277:10064–10072. [PubMed: 11744691]

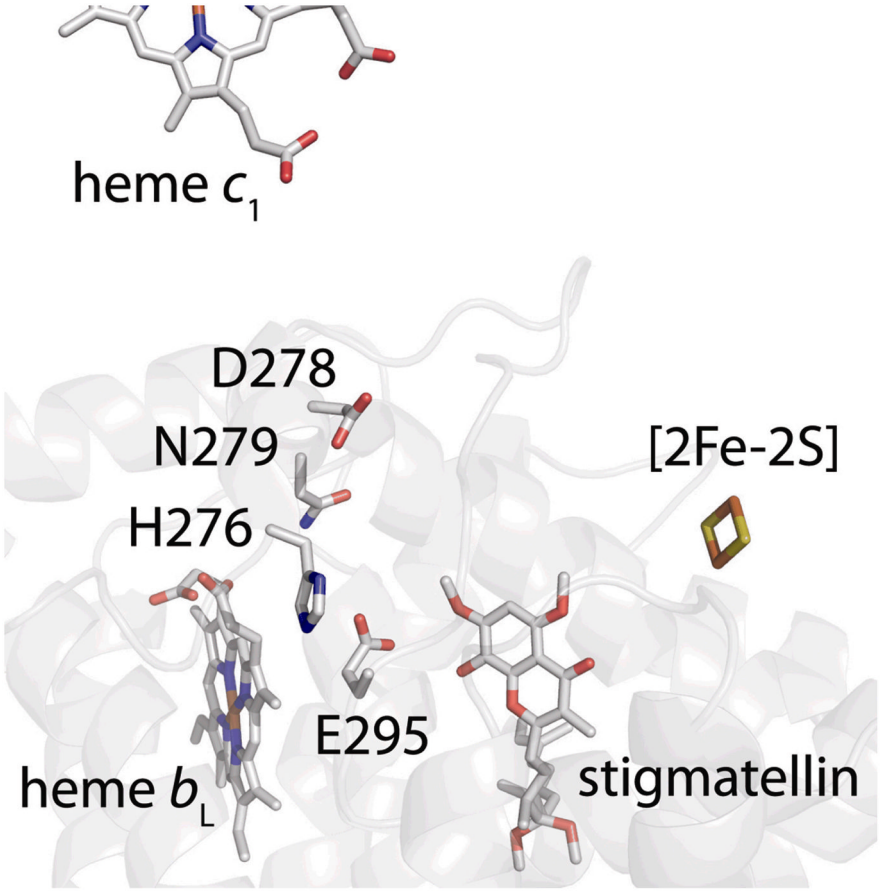

Fig. 1.

A close-up view of the three dimensional structure of the cyt *b* subunit of *R. capsulatus* cyt bc_1 bound with stigmatellin (PDB 1ZRT) (49). For visual convenience, the Fe/S protein and cyt c_1 catalytic subunits are omitted. The cyt *b* subunit in gray is rendered transparent, and its H276, D278, N279 and E295 residues proposed to act as Zn^{2+} ligands (24) are shown in sticks. The [2Fe-2S] cluster, hemes b_L and c_1, and the Q_o site inhibitor stigmatellin are shown as sticks.

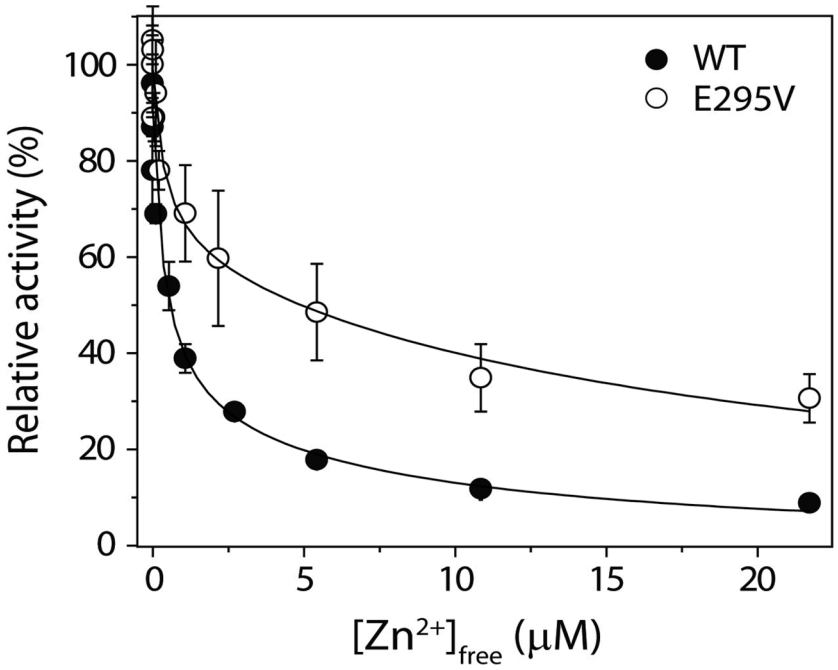

Fig. 2.

Inhibition of purified *R. capsulatus* cyt bc_1 by Zn^{2+}. DBH_2:cyt *c* oxidoreductase activities of the wild-type and E295V mutant enzymes with a $[DBH_2]/[\text{cyt } bc_1]$ ratio of $>10^6$ were assayed at various concentrations of Zn^{2+} in 40 mM Tris-HCl buffer (pH 7.5). Relative wild type and E295V mutant enzyme activities observed in the presence of increasing concentrations of Zn^{2+} are shown with uninhibited 100% activities being approximately 31 and 10μmol of cyt *c* reduced min^{-1} mg^{-1}, respectively (Table 1). The concentration of free Zn^{2+} in the Tris-HCl buffer was obtained as $[Zn]_{free}=[Zn]_o/(1+[Tris]_o/K_{Tris})$ where $[Zn]_o$ and $[Tris]_o$ are the initial concentrations of zinc and Tris, with K_{Tris} = 2.3 ± 0.2 mM (50).

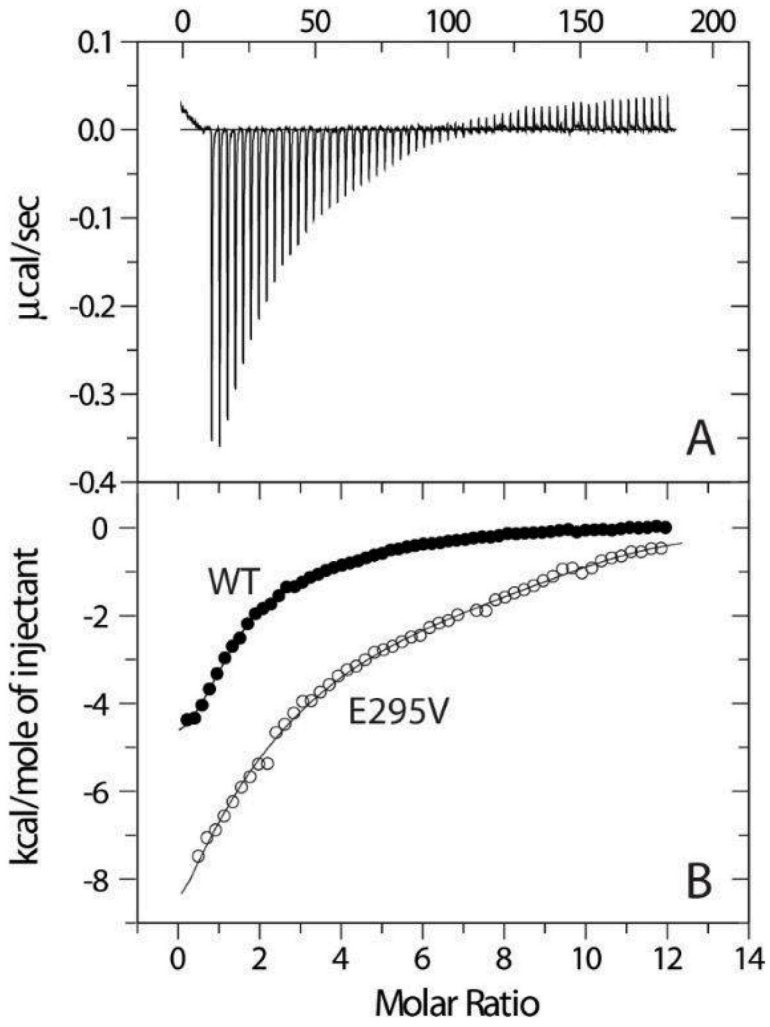

Fig. 3.

Binding of Zn^{2+} to the wild-type and E295V cyt bc_1 as determined by ITC titrations. (**A)** Raw titration data represent the thermal effect of 5 μL injections of 500 μM Zn^{2+} onto a solution of 9.7 μM wild-type enzyme. (**B)** The normalized heat of reaction, derived from the integration of raw data (as those shown in panel *A* for the wild-type), as a function of the Zn^{2+}/cyt bc_1 molar ratio, for the wild-type (black closed circles) and for the E295V mutant (open circles) cyt bc_1 enzymes. The total protein concentrations were 9.7 μM and 11.1 μM for the titrations performed with the wild-type and the E295V mutant enzyme, respectively. The continuous lines represent the best fit of the integrated data to a model that includes two non-interacting sets of binding sites. The corresponding values of the number of sites per protein complex and of the dissociation constants are: $n_1 = 1.13 \pm 0.03$, $K_{D1} = 0.50 \pm 0.07$ μM, $n_2=3.7 \pm 0.2$, $K_{D2} = 6.8 \pm 0.9$ μM for the wild-type and $n_1=1$ (fixed), $K_{D1} = 1.00 \pm 0.36$ μM, $n_2 = 9.1 \pm 0.5$, $K_{D2} = 3.5 \pm 1.6$ μM for the E295V mutant enzymes. See the text for further details.

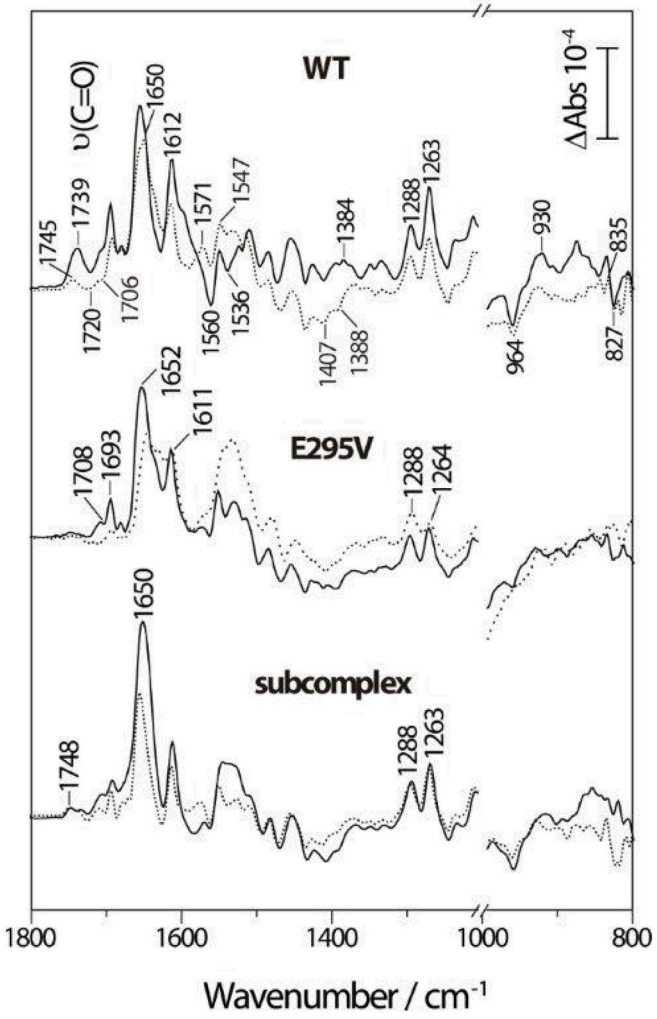

Fig. 4.

Oxidized *minus* reduced FTIR difference spectra of *R. capsulatus* wild-type cyt bc_1 (top), E295V mutant (middle) and cyt b-c_1 subcomplex lacking the Fe/S protein subunit (bottom) enzymes in the absence (solid lines) and presence (dotted lines) of 200 μM Zn^{2+} at pH 8.0. For further details see the text.

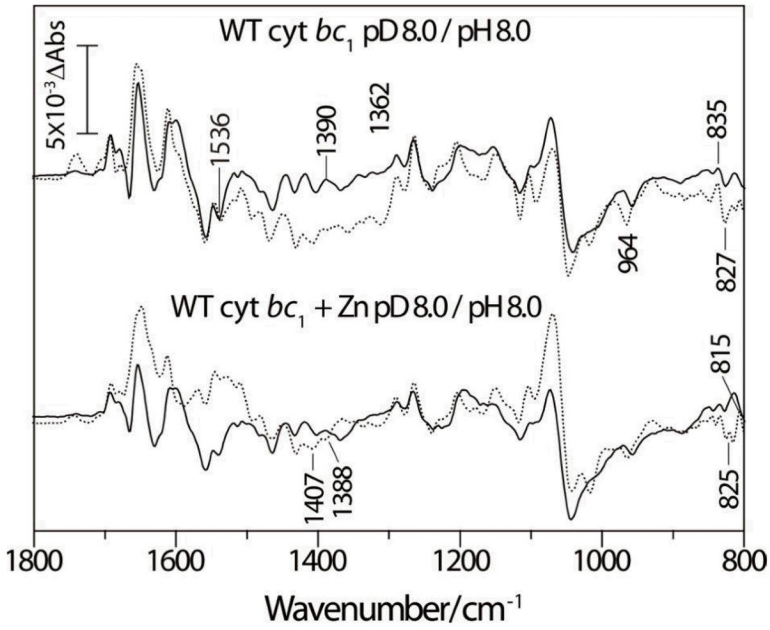

Fig. 5.

The effects of H-D exchange on the FTIR difference spectra of wild-type cyt bc_1 in the absence and presence of 200 μM Zn^{2+}. Top, FTIR difference spectra of the wild-type cyt bc_1 recorded at pD 8.0 (solid line) and pH 8.0 (dotted line). Bottom, FTIR difference spectra of the wild-type cyt bc_1 in the presence of Zn^{2+} recorded at pD 8.0 (solid line) and pH 8.0 (dotted line). See the text for further details.

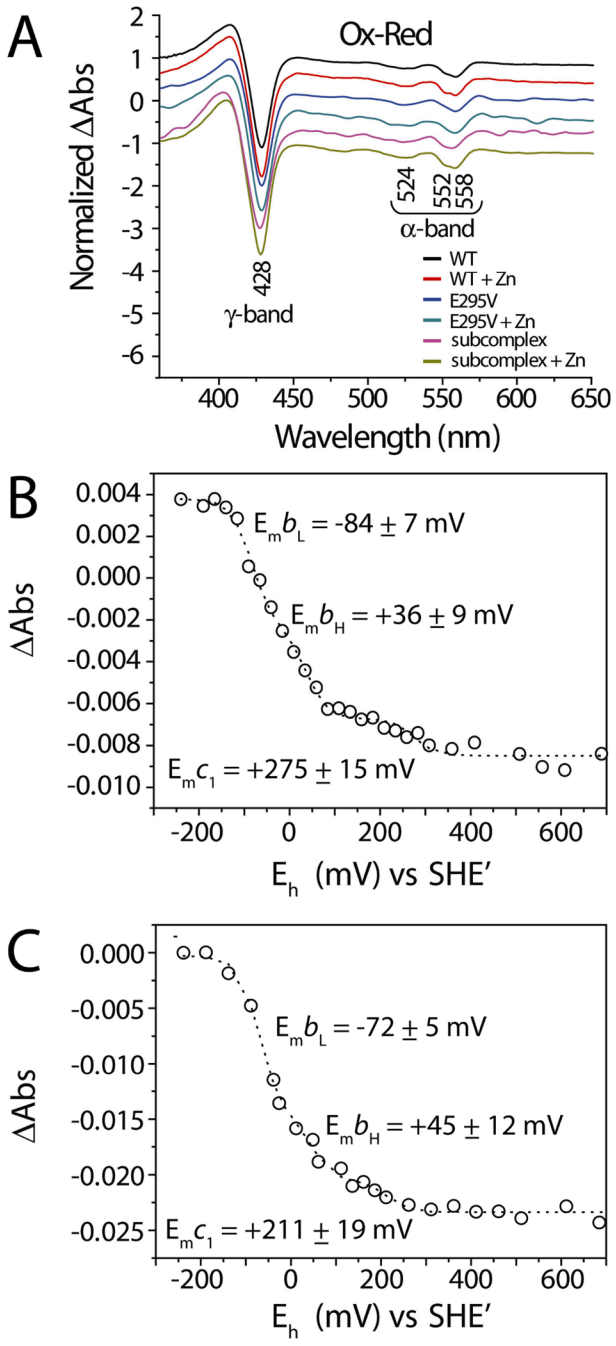

Fig. 6.

Redox midpoint potentials of heme cofactors of wild-type cyt bc_1 in the absence and presence of Zn^{2+}. UV/Vis optical absorbance difference spectra (**A**) of the wild-type, E295V and the cyt b-c_1 subcomplex lacking the Fe/S protein subunit in the presence and absence of 200 μM Zn^{2+}. Voltametric redox equilibrium titrations of heme cofactors of the wild-type cyt bc_1 in the absence (**B**) and in the presence of 200 μM Zn^{2+} (**C**). Potentiometic titrations were performed 100 mM Tris-HCl and 100 mM KCl at pH 8.0. The E_{m7} values for the cyts c_1 and b obtained from the absorption difference in the Soret region (γ band at 428 nm on panel A), and the normalized data were fit to a Nernst equation with three n=1 components. Mediators were used as described for the FTIR studies.

Table 1

Kinetic parameters of cyt bc_1 from *R. capsulatus* and various organisms

Enzyme Source		K_m (μM)	V_{max} (μmol min^{-1} mg^{-1})	K_{cat} (sec^{-1})	V_{max}/K_m (μmol min^{-1} mg^{-1} μM^{-1})	Reference
R. capsulatus[a]	WT	4.9 ± 0.2[b]	42.4 ± 0.8	85.2 ± 13.1	8.6	This study
	E295V	3.1 ± 0.4	10.6 ± 0.4	34.3 ± 4.5	3.4	
S. cerevisiae[a]	WT	6.3	ND	52.1 ± 5.0	ND	(36)
	E272Q	3.2	ND	6.9 ± 1.0	ND	
S. cerevisiae	WT	4	ND	61	(15.3)[d]	(37)
	E272V	4.2	ND	26	(6.2)[d]	

[a] Determined by purified enzyme

[b] Data are means ± standard deviations.

[c] ND, not determined.

[d] Note that these numbers correspond to K*min* (K_{cat}/K_m) as defined in (37) and not to V_{max}/K_m.

Biochemistry. Author manuscript; available in PMC 2011 October 6.

Table 2

Inhibition of purified cyt bc_1 by Zn^{2+}

Enzyme source	K_I (M)	K_D (M)	Complete inhibition (μM)	Reference
Bovine	10^{-7} (pH 7.0)	10^{-7} (pH 7.0) $>2 \times 10^{-6}$	$[Zn^{2+}] > 5$	(39)
Avian	3×10^{-6}	ND	200 (≤ 20%)	(25)
Bacteria	0.9×10^{-6} (pH 7.5)	0.5×10^{-6}	200 (≤ 10%)	This study

ND, not determined.